Earthq Eng & Eng Vib (2019) 18: 719-733 **DOI**: https://doi.org/10.1007/s11803-019-0532-7

Influence of pile spacing on seismic response of piled raft in soft clay: centrifuge modeling

Yang Jun[1,2†‡], Yang Min[3‡§] and Chen Haibing[4‡]

1. *Guangzhou Municipal Engineering Testing Co., Ltd, Guangzhou 510060, China*
2. *School of Civil Engineering and Transportation, South China University of Technology, Guangzhou 510641, China*
3. *Department of Geotechnical Engineering, Tongji University, Shanghai 200092, China*
4. *Institute of Foundation and Structure Technologies, Zhejiang Sci-Tech University, Hangzhou 310018, China*

Abstract: In order to study the influence of pile spacing on the seismic response of piled raft in soft clay, a series of shaking table tests were conducted by using a geotechnical centrifuge. The dynamic behavior of acceleration, displacement and internal forces was examined. The test results indicate that the seismic acceleration responses of models are generally greater than the surrounding soil surface in the period ranges of 2–10 seconds. Foundation instant settlements for 4×4 and 3×3 piled raft (with pile spacing equal to 4 and 6 times pile diameter) are somewhat close to each other at the end of the earthquake, but reconsolidation settlements are greater for 3×3 piled raft. The seismic acceleration of superstructure, the uneven settlement of the foundation and the maximum bending moment of pile are relatively lower for 3×3 piled raft. Successive earthquakes lead to the softening behavior of soft clay, which causes a reduction of the pile bearing capacity and thus loads are transferred from the pile group to the raft. For the case of a 3×3 piled raft, there is relatively smaller change of the load sharing ratio of the pile group and raft after the earthquake and the distribution of maximum bending moments at the pile head is more uniform.

Keywords: piled raft; pile spacing; soft clay; dynamic centrifuge model test; seismic response; subsidence; load sharing; bending moment

1 Introduction

Engineering experiences and research work during the last few decades have proven that the use of piles to reduce raft settlement or considering the contribution of raft to the overall bearing capacity can lead to considerable economic savings without compromising the safety and performance of foundations (Poulos, 2001). In China, piled raft foundations (also known as settlement-controlled composite pile foundations or reducing-settlement pile foundations) have been widely used in a large number of multi-story buildings in deep soft ground. For instance, more than three million square meters of residential buildings (five to seven stories high) have been constructed on piled-raft foundations in Shanghai since the 1990s (Yang, 2000). Long-term field measured data collected for more than 10 years (Tang *et al*., 2014) has shown that piled raft foundations are one of the most economical and sustainable types of pile foundations and the settlement can be satisfied within the allowable settlement value. Pile spacing is the most critical factor affecting the load sharing of pile and raft as well as foundation settlement for most cases. Pile raft foundations generally adopt less piles with much larger pile spacing (more than 6*d*, where *d* denotes pile outside diameter) compared with conventional pile foundations. Due to the very complex pile-soil-raft dynamic interaction effects, the seismic performance of piled raft foundations in soft ground is still unknown, especially when soft ground subsidence occurs. Hence, until now there has not been any reliable seismic design method for piled raft foundations in soft ground for many countries.

When a saturated clay layer is subjected to the cyclic shear during an earthquake, excess pore water pressure is produced, and subsequently, by the dissipation of the accumulated excess pore water pressure, ground subsidence may occur (Matsuda and O-Hara, 1990). Several observations (Scholl, 1989) from past earthquakes (such as the 1976 Tangshan earthquake and the 1985 Mexico earthquake) have shown that the settlements of buildings and structures on soft ground are not only related to the instant subsidence, but also

Correspondence to: Yang Min, Department of Geotechnical Engineering, Tongji University, Shanghai 200092, China
Tel: +86-13901891943; Fax: +86-21-65983388
E-mail: yangmin@tongji.edu.cn
[†]Engineer; [‡]PhD; [§]Professor

Supported by: National Natural Science Foundation of China under Grand No. 41372274
Received September 7, 2017; **Accepted** June 16, 2018

to the reconsolidation settlement caused by the excess pore water pressure dissipation. There are deep soft soil layers widely distributed in the eastern coast of China. In the future, a large number of buildings with shallow foundations or piled raft foundations in these areas have a high probability of being subjected to earthquakes, which could cause large uneven settlement or even collapse. Therefore, the study of seismic response of piled raft foundations on soft ground is currently of great engineering and social significance.

Most of the existing experimental or numerical studies are mainly concerned with the seismic response of piled rafts in dry sand or liquefying soils (Horikoshi *et al*., 2003; Nakai *et al*., 2004; Matsumoto *et al*., 2004; Tang *et al*., 2010; Stringer and Madabhushi, 2013; Tamura and Hida, 2014; Hamada, 2016; Tang *et al*., 2016). Only a few researchers are involved in the dynamic behavior of piled rafts in soft soil through centrifuge and 1g (g denotes acceleration of gravity) tests. Ma *et al*. (2012) investigated the seismic response of the clay pile-raft system with flexible and stiff piles using centrifuge and numerical studies. Banerjee *et al*. (2014) examined the dynamic bending moment of fixed headed piles by using centrifuge tests and numerical modeling. Saha *et al*. (2015) performed 1g shake table tests to study the change in response at different elements of the piled raft supported structure when dynamic soil structure interaction (DSSI) effects are considered. Yang and Yang (2016) carried out two centrifuge-shaking table tests to examine the effects of pile head connection on the seismic acceleration, displacements and load sharing of a friction piled raft-superstructure system in kaolin clay. Zhang *et al*. (2017) performed a series of centrifuge tests on a 4×3 pile-raft system embedded in soft clay to investigate the pile bending moment and raft acceleration response under seismic excitation. Then, Zhang *et al*. (2017) carried out several centrifuge tests and finite element analysis to study the behavior of pile groups in soft clay in the event of the long duration ground motion of about 200 sec strong motion. Meanwhile, there are also some successful reports on the measurements of pile-raft foundations in highly seismic areas such as Japan, Mexico and India. Mendoza *et al*. (2000) recorded the performance of a friction pile box foundation in Mexico City soft soil during the earthquake and yielded valuable information about the foundation performance before, during and after two seismic events. Dash *et al*. (2009) reported the plausible causes of failure of piled raft during the 2001 Bhuj earthquake and concluded that the raft over the nonliquefied crust shared a considerable amount of load of the superstructure and resisted the complete collapse of the building. Hamada *et al*. (2012) monitored the seismic response of a twelve-story base-isolated building using piled raft foundations with ground improvement in an unfavorable soil layer and found that the peak acceleration on the raft was about 60 percent of that of the ground surface due to ground improvement. Yamashita *et al*. (2014) reported and discussed the behavior of settlement and load sharing of piled raft foundations based on the long-term monitoring of several structures and found that no significant changes in foundation settlement or load sharing were observed after the earthquake. Yamashita *et al*. (2016) found that the friction piled raft foundation combined with grid-form cement deep mixing walls showed a good performance in a ground consisting of liquefiable sand and soft cohesive soil under both seismic and static conditions through monitoring a friction piled raft foundation supporting a seven-story building on soft ground.

From the above studies, the analysis of the response of friction piled raft foundations in soft clay subjected to the earthquake is very limited and further investigation is required to improve the understanding of this problem. This work will be of great significance for establishing more reasonable seismic design methods for piled raft foundations or seismic reinforcement of structures located in earthquake-prone areas in the future. In order to investigate the influence of pile spacing on the behavior of friction piled raft foundations in soft ground and to provide the experimental references for further seismic design, a series of dynamic centrifuge tests were carried out on model piled rafts in kaolin clay using the geotechnical centrifuge and shaking table system at Tongji University. A non-homogeneous soft soil with upper overconsolidated clay and lower normally consolidated clay was prepared by the overload effect of the surface sand layer under 50 g centrifuge consolidation. Structural models were simplified to lumped mass and rod member. Two types of pile spacing of 6*d* and 4*d* were considered in two cases. The responses of acceleration, displacement and strain were examined and the contribution of the raft contact with the soil was also investigated. The test results show that the pile-soil-raft interaction makes the dynamic characteristics of the foundation different from the ground surface. The seismic response of the superstructure does not necessarily become worse when using relatively larger pile spacing or fewer piles. The soil resistance beneath the raft base is very beneficial in reducing the uneven settlement of the foundation and dynamic bending moment of pile. For piled raft with larger pile spacing, the load sharing of the pile and the raft is more likely to remain stable before, during and after an earthquake, and the distribution of maximum bending moment at the pile head for different piles will be more uniform.

2 Centrifuge tests set-up

2.1 Testing equipment

All the centrifuge experiments in the present study were carried out at 50 g on the TLJ-150 geotechnical centrifuge at Tongji University (Ma *et al*., 2006). The 3 m radius centrifuge has a payload capacity of 150g-tonnes

and can spin up to a maximum acceleration of 200 g. The shaking table has a maximum vibration acceleration of 20 g, maximum duration of 1 s and vibration frequency of 20–200 Hz at 50 g of centrifuge acceleration. In order to minimize the effects of boundary reflection and inertial loading, a laminar shear model box was used in the test, which consists of 22 high-strength hollow aluminum rings (each having a thickness of 2.5 cm) and uses a rubber membrane inside. The internal dimensions of the model box are 500 mm length by 400 mm width by 550 mm height. In the perimeter there are four drainage holes connected with internal permeable stone at the bottom. This configuration is beneficial in implementing double-sided drainage consolidation for soft clay (see Fig. 1).

2.2 Soil sample

A medium sand layer with a thickness of 20 mm was first paved into the base of the model box. The mixture of kaolin clay powder and water (at a water content of 1.5 times the liquid limit) was poured in the model box. The physical parameters of kaolin clay are listed in Table 1. A filter paper was paved on the surface of the clay layer, and then a dry medium sand layer was poured at a uniform rate until its thickness reached 30 mm, which corresponded to an effective overburden stress of about 23 kPa at the top of the clay mixture. The sample, shaker and other accessories were installed to the centrifuge.

After the above work was completed, the clay mixture was subjected to self-weight consolidation at 50g under double drainage until the consolidation degree of the kaolin clay layer was more than 90%. According to Terzaghi's one-dimensional consolidation theory, the time required to complete consolidation of the kaolin clay layer is more than 22 h (about 6.4 years in prototype time). In order to accurately control this process, the laser displacement sensor is applied to measure the settlement of the soil surface and the pore water pressure sensor monitors the dissipation of the excess pore water in soft clay. When the soil settlement rate slows down or the pore water pressure tends to be stable over a period of time, the centrifuge consolidation is considered to be complete.

After in-flight centrifuge consolidation of clay was completed, the top sand layer and filter paper were removed. A T-bar test was performed to measure the clay strength profile at 50 g. Existing centrifuge and field tests showed that the penetration resistance obtained with equal velocity penetration was the smallest. The faster the penetration rate, the more significant the penetration resistance due to the viscous effect. The relatively better estimated strength values were obtained when the penetration rate of 1–2 mm/sec was in remolded soft clay (Bemben and Mayers, 1974; Chung *et al*, 2006). The penetration rate used in these tests is 1.3 mm/sec. The relationships between undrained shear strength s_u of kaolin clay and soil depth from the T-bar test for both tests are shown in Fig. 2. It is seen that the strength of the soil with the longest distance from the upper and lower drainage boundaries is lowest compared with that at other depths. The increase of upper soil strength (at overconsolidation conditions) is mainly related to

Table 1 Physical parameters of kaolin clay

Property	Value
Specific gravity, G_s	2.67
Mean grain size, D_{50} (mm)	0.038
Bulk unit weight, γ (kN/m^3)	16.4
Water content, w (%)	69
Void ratio, e	1.73
Liquid limit, w_L (%)	54
Plastic limit, w_P (%)	26
Plasticity index, I_P (%)	28
Coefficient of consolidation (at 100kPa), c_v (m^2/a)	12.5
Coefficient of permeability (at 100kPa), k (cm/s)	1.13×10^{-7}

Fig. 1 Laminar shear model box

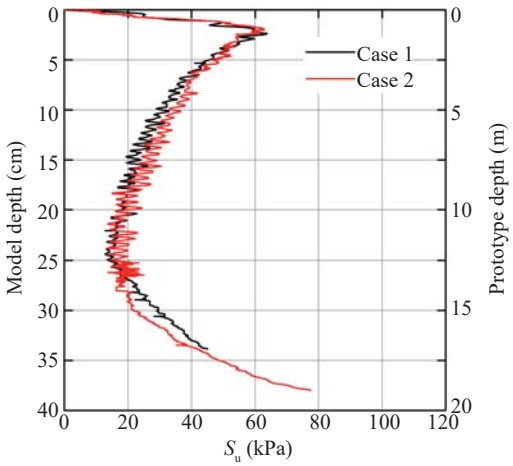

Fig. 2 Undrained shear strength of kaolin clay from T-bar tests

the overloading effect of the pre-laid sand layer during centrifuge consolidation. Due to the presence of the drainage sand layer at the base and the weight of the soil layer, s_u increases rapidly along the depth. Comparing the shear strength of the upper soil and the total weight of the structure and foundation model, it can be seen that the soil under the raft meets the requirements of bearing capacity, and the pile beneath the raft is mainly used to control the foundation settlement.

2.3 Model configuration and test program

As summarized in Table 2, two dynamic centrifuge model configurations (Case 1 and 2) were performed independently with several artificial earthquake events. Two piled raft models were installed at 1 g (after the completion of centrifuge consolidation). Except for the acceleration amplitudes, other parameters (such as frequency content and the duration) are identical for the three earthquake ground motions in the two cases. Each earthquake event was separated by a period of time (more than 50 days after each earthquake, approximately more than a 90% re-consolidation ratio) for dissipation of excess pore water pressure induced by shaking and the settlements of the piled raft model and ground surface can be observed. Model materials, dimensions and sensor placement are consistent between the two cases except for the pile spacing. The superstructure masses, the heights from the raft top and their fixed-base periods are given below.

Figure 3 presents sketches of the laminar model box, piled raft-superstructure models, soil profiles, and instrumentation used in the tests. Five accelerometers (A1~A5) arranged at various locations are used to measure the seismic acceleration of soft clay, foundation and superstructure. P1 and P2 represent pore water pressure sensors. Seven displacement transformers (LS1~LS4 and LV1~LV3) are used to scan the time history of displacement of the model and soil box at different times. Strain gauges are attached to model pipe piles at various levels to measure the axial force and bending moment. All sensors are connected to the centrifuge data acquisition system. According to the requirements of centrifuge consolidation and dynamic tests, the channel sampling frequency is set to 1 Hz and 5000 Hz, respectively. More detailed information about the sensors used in the tests are listed in Table 3. Compared with existing dynamic centrifuge tests of piled raft (see Banerjee *et al*., 2014; Hamada, 2016 and Zhang *et al*., 2017a; 2017b), the arrangement of the piled raft model and soil box is reasonable enough to prevent significant boundary effects.

Figure 4 shows the geometric dimensions of the raft model, the position of the pipe piles and four columns. Except for the material (steel) used in the model superstructure and the column, raft and pile model are made of aluminum. Each pile and column are rigidly fixed to the raft with bolts, which can be considered as the rigid connection. According to the similarity relationship of the centrifuge test, the model and prototype size similarity ratio is 50 with 50 g centrifuge acceleration (Schofield, 1981). The difference in deformation mechanisms of different members will affect the physical quantity similarity control. The piles and columns under the horizontal seismic loads are mainly controlled by the bending stiffness. The raft and superstructure are mainly controlled by the mass and the lateral moment of inertia. Hence, the aluminum pipe

Table 2 Summary of dynamic centrifuge test program

Test identification	Pile spacing, s	Pile number	Structure properties, T(s)*	a_{max}
Case 1-1st	6d	9	0.44	0.06 g
Case 1-2nd	6d	9	0.44	0.10 g
Case 1-3rd	6d	9	0.44	0.23 g
Case 2-1st	4d	16	0.44	0.05 g
Case 2-2nd	4d	16	0.44	0.11 g
Case 2-3rd	4d	16	0.44	0.24 g

Note: T denotes the natural period of superstructure under fixed base condition. a_{max} denotes the actual maximum acceleration output of shaker measured at the base. Mass of superstructure: 40772 kg; Height of superstructure: 6.0 m; mass of raft: 61210 kg. All measurements presented have been converted to prototype units.

Table 3 Detailed information about sensors used in tests

Sensor	Type	Measuring range	Sensitivity
Accelerometer (A)	PCB 352C65	±50 g	100 mV/g
Differential displacement meter (LV)	CW-100	±50 mm	38 mV/mm
Laser displacement sensor (LS)	CP24MHT80	40~160 mm	83 mV/mm
Pore water pressure sensor (P)	HC-25	0~500 kPa	0.1 mV/kPa

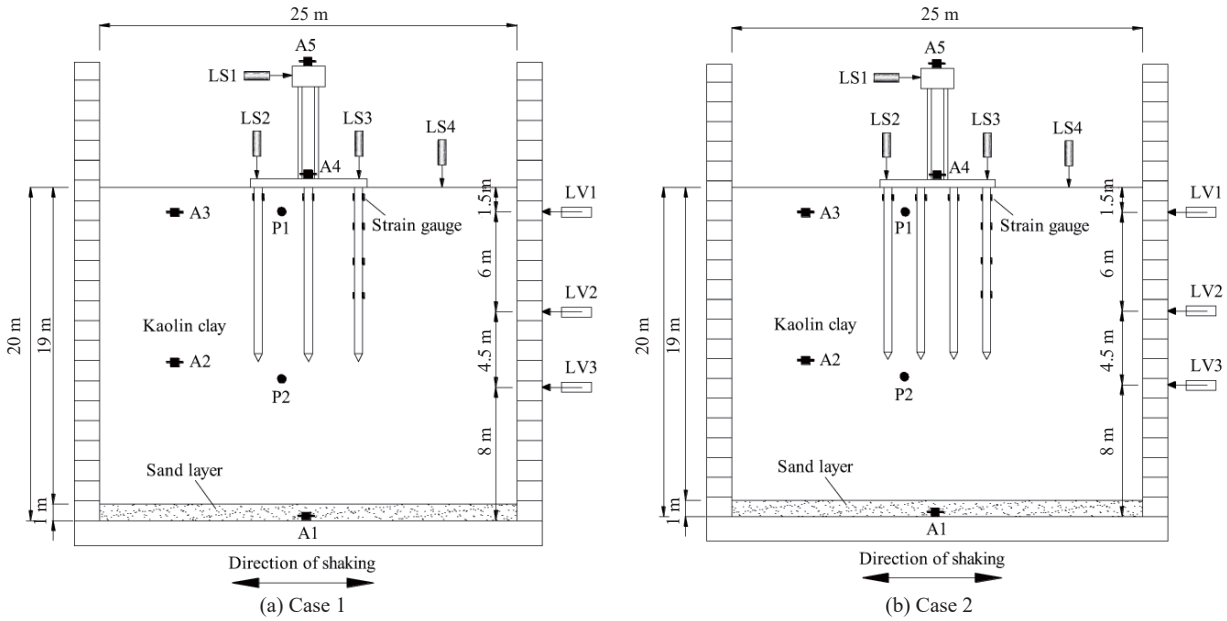

Fig. 3 Model setup and sensor locations (on prototype)

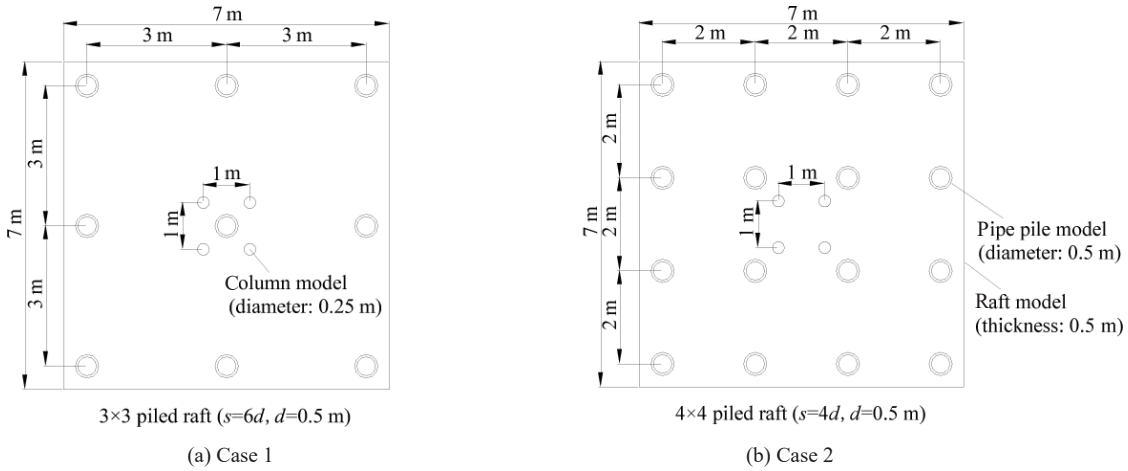

Fig. 4 Raft dimension and pipe pile position (on prototype)

pile had a flexural stiffness (*EI*) of 127 MN·m^2, which is approximately equivalent to 0.5 m diameter steel pipe pile with 14 mm wall thickness. The flexural stiffness (*EI*) of four columns was 643.9 MN·m^2. The masses of the raft and superstructure on the prototype were 61,210 kg and 40,772 kg, respectively. More detailed information about similarity relationships of the model and prototype is given in Table 4.

Figure 5 presents photos of the piled raft and superstructure models in the two tests. The model system includes simplified superstructure, columns, rafts and pipe piles. All strain gauges attached to model piles were connected in full-bridge circuit to guarantee accuracy. The bending moment and the axial force of the model pile were calibrated by step-by-step loading according to the cantilever beam and axial compression rod, respectively. Then, the relationship between the strain and internal forces of the model pile can be obtained.

2.5 Input seismic motion

The input seismic motions used in the experiments were generated from artificial seismic data with major duration of about 30 sec, as recommended in the Code for Seismic Design of Buildings in Shanghai (2013), which was obtained from the strong earthquake database of the Pacific Earthquake Engineering Research (PEER) and the KiK-net digital strong earthquake recording system of the Institute of Disaster Prevention Science and Technology of Japan. The target response spectrum and the site conditions of the Shanghai area are both considered. Due to the requirements of the centrifuge test similarity ratio and output vibration frequency of the shaker, the prototype seismic wave is scaled by time and amplitude by using a filtering process. The acceleration time histories for the input and generated earthquake events with peak ground acceleration (a_{max}) of about

Table 4 Similarity relationship of piled raft models used in tests

Name	Properties	Model level	Prototype level
Pile	Outside diameter (m)	0.01	0.50
	Wall thickness (m)	0.001	0.014
	Modulus (GPa)	70	206
	EI (N·m^2)	20.3	1.27×10^8
	Similarity ratio of EI	1	50^4 (50^4)
	EA (N)	1.98×10^6	4.28×10^9
	Similarity ratio of EA	1	46.5^2 (50^2)
Column	Diameter (m)	0.005	0.25
	Modulus (GPa)	210	210
	EI (N·m^2)	103.03	643.9×10^6
	Similarity ratio of EI	1	50^4 (50^4)
Raft	Width (m)	0.14	7.00
	Thickness (m)	0.01	0.50
	Density (kg/m^3)	2700	2500
	Weight (kg)	0.53	61210
	Similarity ratio of m	1	48.7^3 (50^3)
Superstructure	Volume (m^3)	4.5×10^{-5}	5.625
	Density (kg/m^3)	7850	2500
	Weight (kg)	0.353	40772
	Similarity ratio of m	1	48.7^3 (50^3)

(a) Case 1 (b) Case 2

Fig. 5 Photos of piled raft and superstructure model

0.100 g are shown in Fig. 6(a) in prototype terms. It can be seen that the generated waveforms of the shaking table are generally consistent with the input motion. Figure 6(b) shows the Fourier amplitude spectrum of the acceleration on the shaking table. It can be seen that the low frequency component distributes in most frequency ranges. Six peak values (seeing P-1 ~ P-6), mainly located in the range of 0.1–2 Hz, correspond to the frequencies of 0.18 Hz, 0.26 Hz, 0.32 Hz, 0.56 Hz, 0.99 Hz and 1.85 Hz, respectively.

3 Test results and discussion

The prototype scale is used in the following discussion.

3.1 Verification of boundary effect of laminar shear box

In order to verify the flexible boundary simulation effect of the laminar shear box, the free-field site

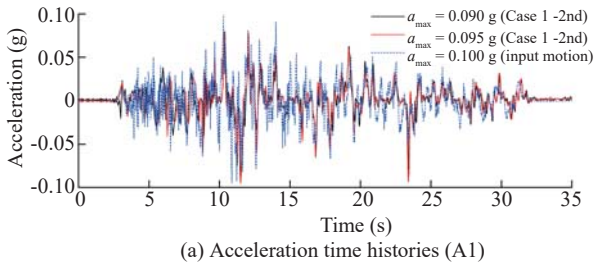

(a) Acceleration time histories (A1)

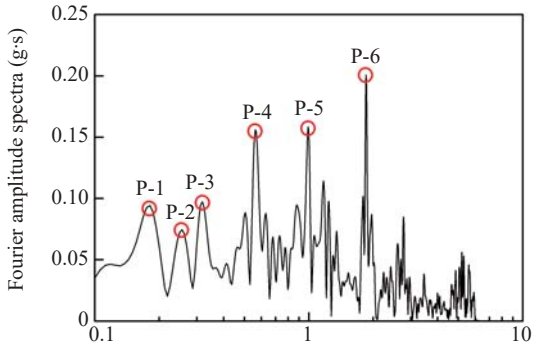

(b) Fourier amplitude spectrum

Fig. 6 Input seismic waves used in dynamic centrifuge tests

analysis software DEEPSOIL (Hashash *et al*., 2015) was used to compare the consistency of the calculated and measured acceleration time histories at different depths. In this study, the dynamic response of soft clay was simulated by an equivalent linear model (see Hardin and Drnevich, 1972). As shown in Fig. 7, the soil shear modulus ratio G/G_{max} decreases and the damping ratio λ increases as the cyclic shear strain γ_c increases. The maximum shear modulus G_{max} and damping ratio λ are usually determined by resonance column and dynamic triaxial tests. The relationship between γ_c and G/G_{max} as well as λ proposed by Vucetic and Dobry (1991) was used to consider the effects of soil plasticity and the overconsolidation ratio.

Assuming that the bottom of the soft clay is fully rigid, the acceleration measured at this position was taken as the model input to calculate the seismic acceleration at different depths. Figure 8 shows the measured and calculated acceleration time history curves located in

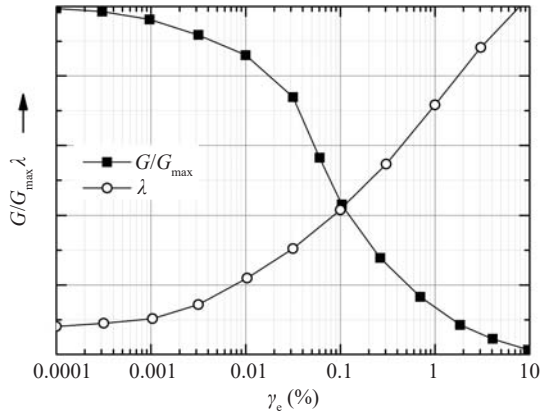

Fig. 7 Relationship of cyclic parameters and cyclic shear strain

the middle and near the surface of the soft clay under the input ground motion (a_{max} = 0.09 g) in Case 1. Although there are some slight gaps, the calculated and measured results are generally consistent and the spectral components are closer, indicating that the measured soil dynamic responses are similar to the free field motion and the effect of the laminar shear box simulating the seismic problem of soft ground is encouraging.

3.2 Earthquake acceleration

Acceleration time histories of soft clay at different depths in Case 1-2nd and Case 2-2nd are shown in Fig. 9. From the results of the measured acceleration, it can be observed that the peak acceleration decays gradually from the base of the model box to the soil surface, because the soft ground with low natural frequency has generally a reduction in acceleration.

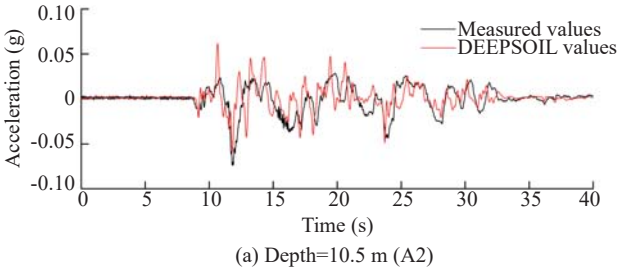

(a) Depth=10.5 m (A2)

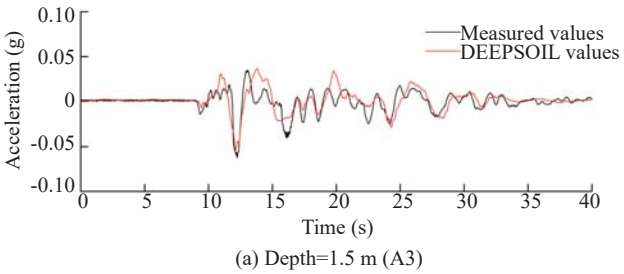

(a) Depth=1.5 m (A3)

Fig. 8 Acceleration time histories of soft clay (Case 1-2nd)

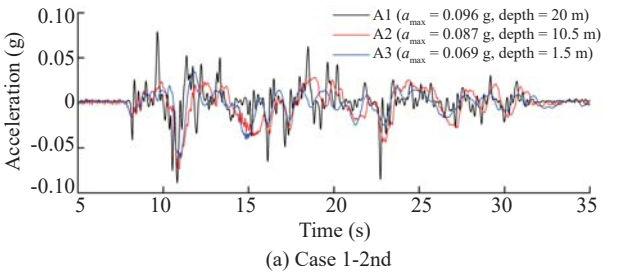

(a) Case 1-2nd

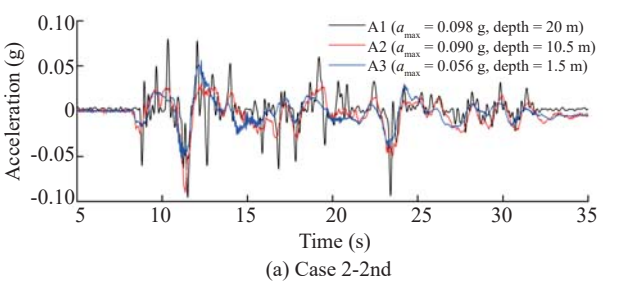

(a) Case 2-2nd

Fig. 9 Acceleration time histories of soft clay layer (Case 1-2nd)

Figure 10 shows the Fourier amplitude spectrum of the acceleration located at different depths for two cases subjected to the second ground motion. The high-frequency components of the output movement of soil in the middle and at the surface are suppressed. The low-frequency components are magnified and the magnification is most significant in the middle depth of the soil layer. This is due to the fact that before dynamic tests, the strength of soft clay in the middle depth is lower than the base and the surface (refer to Fig. 2). It is more prone to softening when subjected to horizontal seismic motion at this position. The acceleration of soil surface is significantly amplified at three frequency components but decreases at other frequency ranges, which indicates that the natural frequency of soft ground in the experiments is near 0.2–0.4 Hz. Banerjee *et al*. (2007) found that the soft soil acceleration was generally amplified as the seismic wave propagates from base to surface, which is inconsistent with the present tests. There may be two reasons for this. First, the soil used in this study is in the overconsolidated state, which has different stress and strain behavior when compared with the normally consolidated clay. Second, the thickness of soft clay in this study is relatively smaller, which may cause the high-frequency component energy of the seismic input wave to decay more quickly than the low frequency in the thicker soil layer.

Figure 11 shows the ratio of spectral acceleration of the raft to the soil surface (damping ratio of 5%). Due to the dynamic piled-soil-raft interaction, the acceleration responses of the raft and surrounding soil surface are not exactly the same. Regardless of the pile spacing used, the spectral acceleration of the raft exceeds the soil surface in a wider range of period. Due to the increase of frequency and level of input seismic motion, the soil strength gradually decreases and the natural period of soft ground is prolonged. The period corresponding to the maximum ratio of raft to soil surface also increases from 1–3 s (for the first motion) to 3–5 s (for the second motion), and then continues to increase to 8 sec and more (for the third motion). From this point of view, ignoring the influence of dynamic soil-structure interaction on the seismic response of the foundation in soft ground may cause the seismic design of the piled raft to be unsafe, especially for high-rise buildings or structures with much longer periods.

In order to compare the influence of different pile spacing on the dynamic characteristics of the superstructure, the ratio of spectral acceleration of the superstructure to the soil surface (damping ratio of 5%) is plotted in Fig. 12. For both tests, when the level of the input motion is small (such as the first motion), the rocking of the superstructure amplifies significantly in a shorter period. With the increase of ground motion level, the period range of amplification significantly is beginning to extend. Comparing the results from three earthquakes, it can be found that the spectral acceleration ratios for Case 2 (s=4d) are greater than Case 1 (s=6d) in

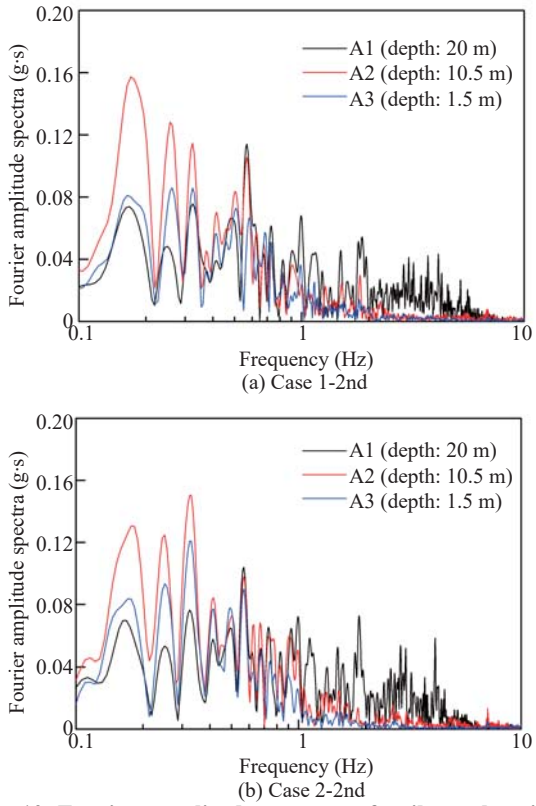

Fig. 10 Fourier amplitude spectra of soil acceleration at different depths

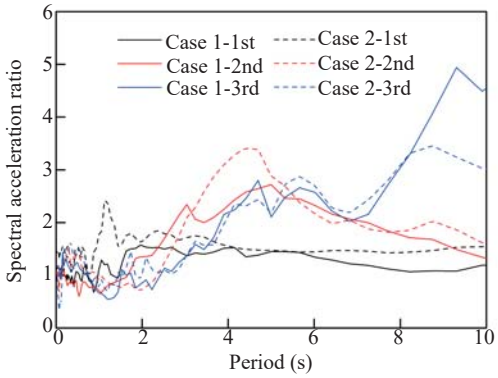

Fig. 11 5% damped acceleration response spectra ratio of raft to soil surface

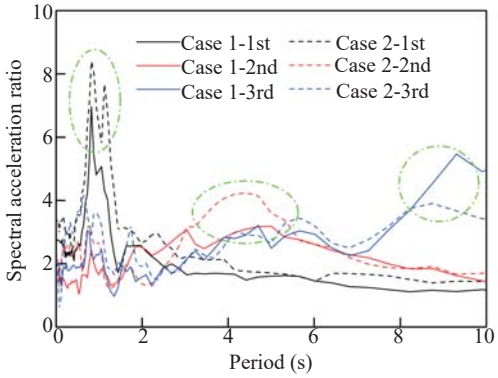

Fig. 12 5% damped acceleration response spectra ratio of superstructure to soil surface

most period ranges (except the period of 8 sec and more for the third ground motion).

Although the base input acceleration cannot be exactly the same, the difference of input acceleration time-histories is generally insignificant. Figure 13 shows the acceleration time histories of superstructures measured through A5 in two cases. It can be seen that the acceleration amplitude for Case 1 (s=6d) is smaller than Case 2 (s=4d) most of the time for three input seismic motions. As the level of the ground motion is increased, the acceleration gap between the two cases becomes more significant. The results indicate that the horizontal vibration of the superstructure does not necessarily have an impact when using larger pile spacing. This is probably because when larger spacing is used, the vertical restraint effect of the soil on the raft is more significant, which helps to improve its ability to resist the horizontal shear force and ease the inertial motion of the superstructure.

3.3 Soil horizontal displacement and excess pore water pressure

Figure 14(a)–(c) shows the soil horizontal displacements recorded on the side of the shear model box for case 1. The horizontal displacement of the soil surface (LV1) has more pronounced changes than the other positions (LV2 and LV3), which is related to the smaller vertical stress of the shallow soil layer.

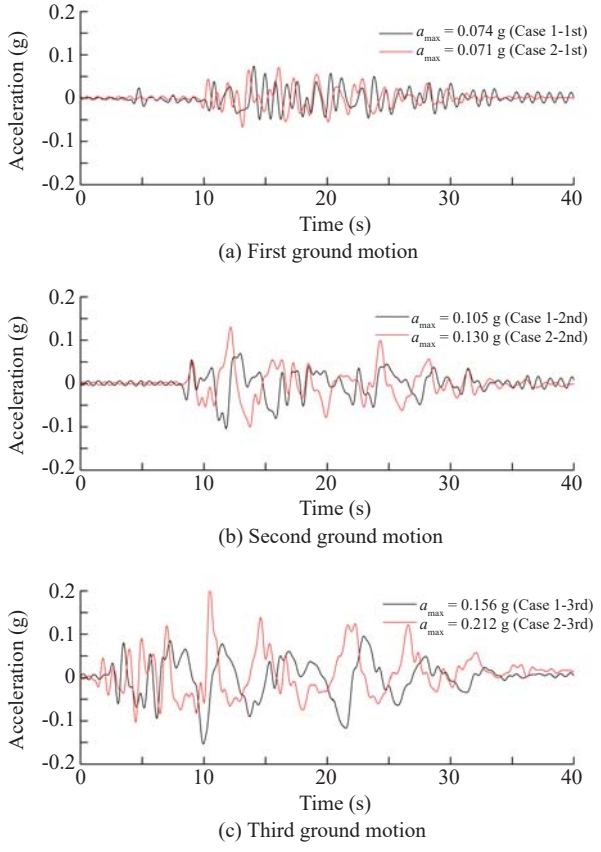

Fig. 13 Acceleration time histories of superstructure during three earthquakes

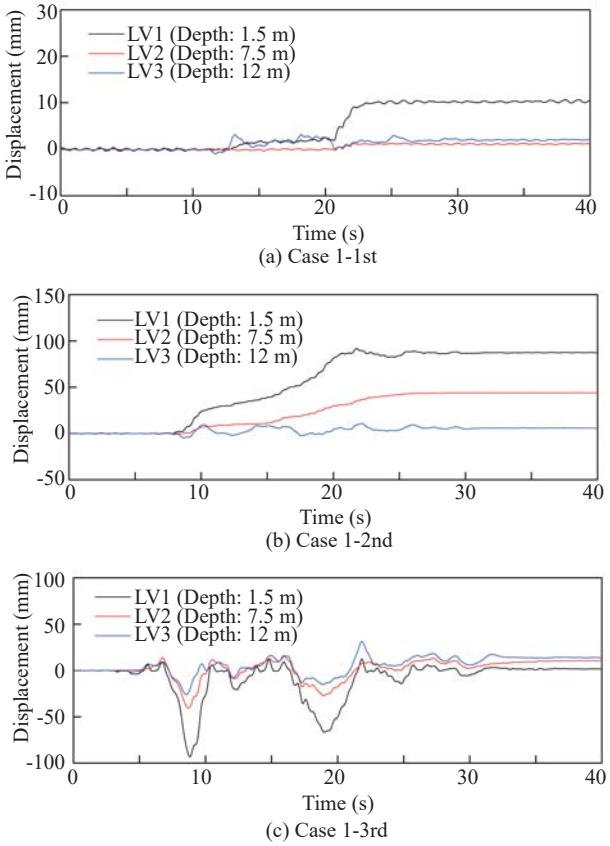

Fig. 14 Horizontal displacement of soft clay layer during three earthquakes

However, the fluctuation is more significant in the third seismic motion, where the horizontal displacements of soft soils at different depths gradually accumulate during the earthquake.

Figure 15 shows the time histories of excess pore water pressure (EPWP) measured beneath the raft base during the three earthquakes. The EPWP in the soft clay slowly increases with the earthquake process and remains constant when the earthquake ceases, which is related to the lower permeability of kaolin clay. The degree of increase of pore water pressure in soft clay is very limited, the maximum EPWP is not more than 3 kPa, and the pore water pressure for spacing of 6d is larger than that of 4d; this can probably be attributed to the shielding effect of piles on the soil motion under the horizontal earthquake, and is more significant when the pile spacing is smaller.

3.4 Instant and post-earthquake displacements

Figure 16 shows the lateral displacement time histories of the superstructure during three earthquakes. The measured lateral displacement time histories of the superstructures are very similar for both cases. For the first and second seismic motions, the residual lateral displacements of superstructures are very close to each other. However, at the end of the third earthquake, the residual lateral displacement for Case 1 (s=6d) is not

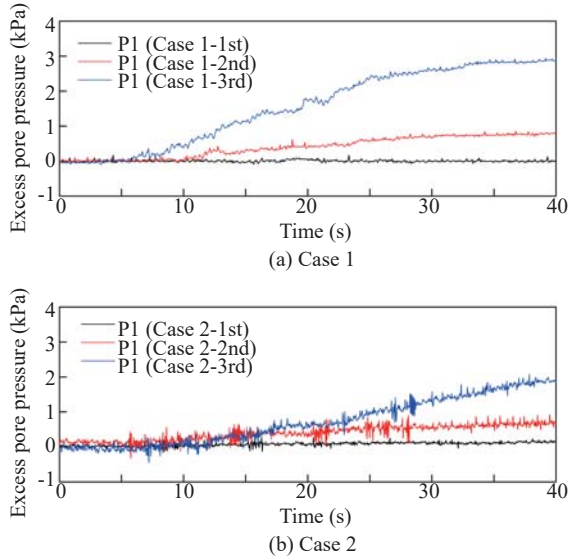

Fig. 15 Excess pore water pressure during three earthquakes (Depth: 1.5 m)

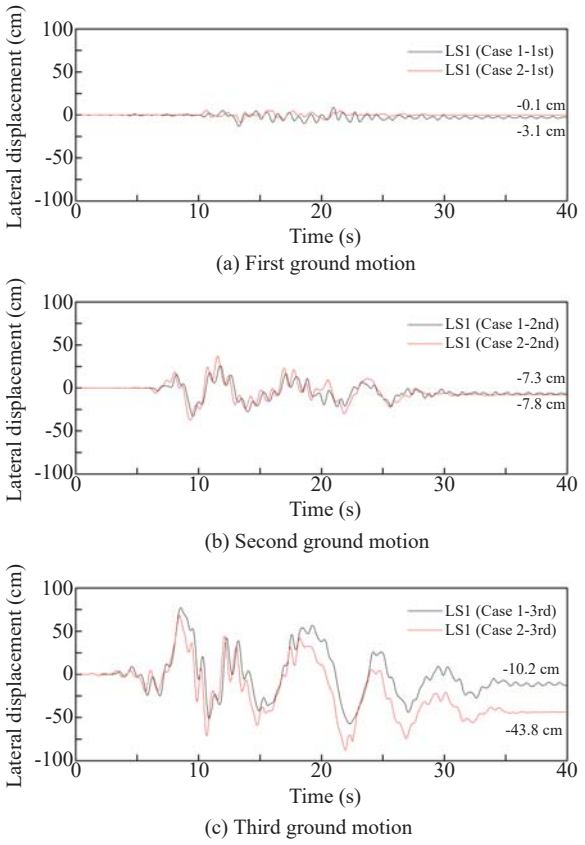

Fig. 16 Lateral displacements of superstructure during three earthquakes

more than 1/4 of Case 2 (s=4d). This is because the stiffness softening of the kaolin clay is not significant at the lower seismic level (for the first two shakings). The soil has enough resistance to inertial motion and rocking of the piled raft foundation. While under the stronger seismic motion, the natural period of the soft clay and structural system have lengthened and are close to each other over a wider range due to the nonlinear properties of soft clay, which induces larger horizontal displacements in the two cases. In addition, the natural period of the piled raft - superstructure system is much closer to that of the soft ground, which may be the reason that residual displacement for Case 2 is much larger than for Case 1 in the third motion.

Figure 17 shows the instant settlements during the three earthquakes. The raft settlement (average value (A. V.) of LS2 and LS3 measurement) and the soil surface settlement (measured by LS4) increase with the earthquake intensity. In Case 1, the total stiffness of the piled raft foundation is lower than Case 2 because fewer piles are used, which induces greater instant settlement during the three earthquakes. However, the settlement difference in the two cases under similar seismic motion is still small, which illustrates that the contact between the raft and the soil plays a positive role in reducing foundation instant settlement.

Figure 18 shows photos of the piled raft in the model box before and after the earthquake for Case 2 (s=4d). After going through three earthquakes, the raft top elevation is lower than the surrounding soil surface and the foundation inclines to one side (seeing Fig. 18(b)), which is in sharp contrast with that shown in Fig. 18(a). It is due to the fact that the soft clay under the raft is subjected to the horizontal seismic force and the additional force from the superstructure and the raft, which induces the EPWP to be higher than that of the surrounding free-field soil. Furthermore, the input seismic wave is not completely symmetrical, causing the structure eccentricity to gradually accumulate as the

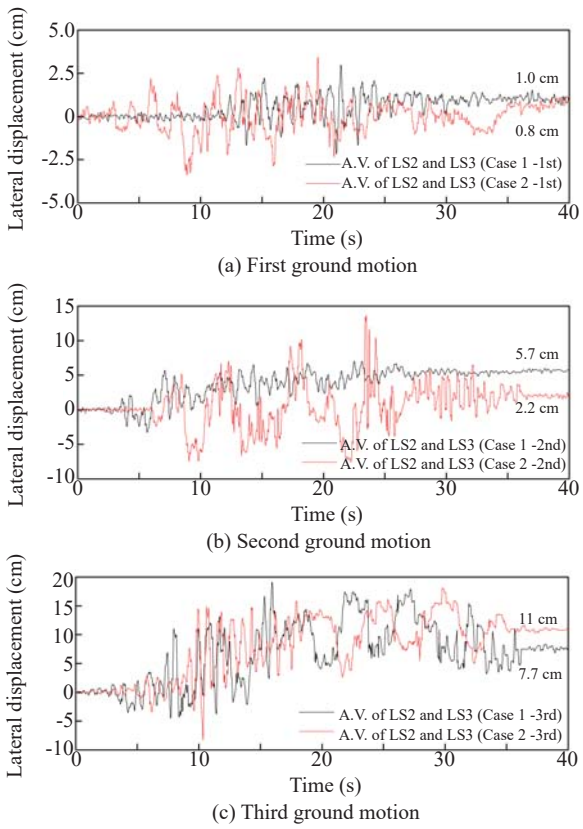

Fig. 17 Instant settlements during three earthquakes

(a) Before dynamic centrifuge tests

(b) After dynamic centrifuge tests

Fig. 18 Photos of piled raft in the model box (Case 2)

number of earthquakes increases. As a result, the raft shows a more pronounced non-uniform subsidence than the surface of the surrounding soil. Due to the excess pore water pressure caused by the earthquake, it can be observed that water is seeping in the vicinity of the raft, on the lower surface and in the crack of the soil.

Table 5 summarizes the settlement and inclination after each earthquake in the two cases. Raft settlements generally exceed the settlement of the free-field soil surface, which is caused by the inertial forces of the superstructure and foundation. It can be also seen that the difference between the residual deformation (including average settlement and inclination) of the rafts for two cases increases after each earthquake as the seismic intensity increases. In stronger seismic events (such as the second and third seismic motions), the degree of raft inclination for Case 1 is much less than that for Case 2.

The long-term settlements of rafts (A.V. of LS2 and LS3 measurement) for two cases are also recorded for a period of time (50 days) after each earthquake. It can be seen from Fig. 19 that the settlements of the piled rafts continues to increase as the excess pore water pressure dissipates, which was induced by the earthquake. As a result of using more piles to support loads from the structure and the raft, the piled raft foundation for Case 2 has higher vertical stiffness and its average settlement is generally smaller than Case 1.

Table 6 shows the long-term settlements after each earthquake in the two cases. Compared with the

Table 5 Residual settlement and inclination of models after each earthquake

Measured content	Measured time	Test identification	
		Case 1	Case 2
Average settlement of raft (cm)	After 1st motion	1.0	0.8
	After 2nd motion	5.7	2.2
	After 3rd motion	7.7	11.0
Settlement of soil surface (LS4 measurement) (cm)	After 1st motion	0.4	0.3
	After 2nd motion	2.0	1.8
	After 3rd motion	4.4	3.6
Raft inclination	After 1st motion	0.002	0.000
	After 2nd motion	0.003	0.016
	After 3rd motion	0.009	0.042

Note: Raft inclination denotes the ratio of settlement difference on both sides of raft top to the horizontal distance of the measured points.

Table 6 Long-term settlements of models after each earthquake

Measured content	Measured time	Test identification	
		Case 1	Case 2
Average settlement of raft (cm)	50 days after 1st motion	3.0	1.0
	50 days after 2nd motion	3.4	2.3
	50 days after 3rd motion	6.8	1.1
Settlement of soil surface (LS4 measurement) (cm)	50 days after 1st motion	2.4	2.1
	50 days after 2nd motion	3.2	2.5
	50 days after 3rd motion	4.0	4.3

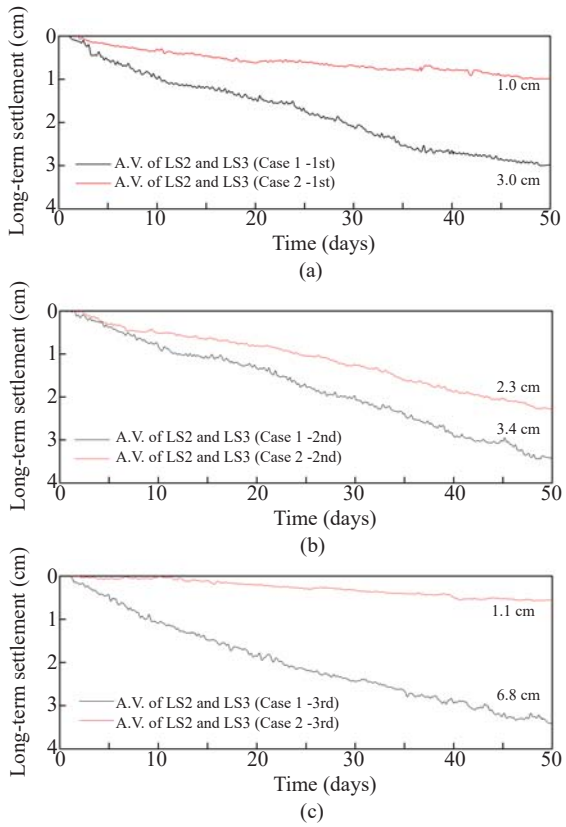

Fig. 19 Long-term settlements after three earthquakes

settlement of the soil surface, the average settlement of the raft is larger in Case 1 while the results are the opposite in Case 2. It indicates that when using more piles or smaller spacing, the settlement rate of the piled raft system is slower than that of the free-field soil surface for a long time after each earthquake. This may induce negative friction on the model pile shafts (or increase pile axial force), which will adversely affect the bearing behavior of the foundation system when using conventional design methods based on bearing capacity (without considering earthquake - induced ground consolidation settlement).

3.5 Vertical load sharing of pile and raft

Load sharing of the pile and the raft is of great concern to designers and engineers, especially the way load transfers before and after the earthquake for the pile design principles based on settlement control. Table 7 shows the pile group (PG) load and the load sharing ratio of PG estimated from measured axial strains of model piles in different experimental stages. When subjected to horizontal input seismic motion, the horizontal shear strain of soft clay causes the softening behavior of soil. The bearing capacity and stiffness of the piled raft foundation are reduced after the earthquake. It can be observed that some loads transfer from the pile group to the raft at the end of each seismic motion, and the changes in the load sharing ratio for Case 2 are more significant than Case 1. It is due to the fact that more piles are used in Case 2 than Case 1, which will induce much greater reduction of the pile group under the same seismic motion, which is consistent with existing experimental results and site measurements (Horikoshi *et al*., 2003; Yamada *et al*., 2001; Yamashita *et al*., 2014). Furthermore, following the soil reconsolidation process and the dissipation of excess pore water pressure, the shear strength of soft clay is partially recovered. Hence, the load sharing ratio of the pile group begins to increase slightly within 50 days after the end of the earthquake.

Table 7 Load sharing ratio of pile and raft before and after the earthquake

Test identification	Experimental stage	PG load (kN)	LSR of PG (%)	Change of LSR (%)
Case 1	Before 1st motion	506	46.0	
	End of 1st motion	494	44.9	-1.1
	After 50 days	501	45.5	0.6
	End of 2nd motion	459	41.7	-3.8
	After 50 days	495	45.0	3.3
	End of 3rd motion	394	35.8	-9.2
	After 50 days	445	40.5	4.7
Case 2	Before 1st motion	842	76.5	
	End of 1st motion	812	73.8	-2.7
	After 50 days	821	74.6	0.8
	End of 2nd motion	701	63.7	-10.9
	After 50 days	708	64.4	0.7
	End of 3rd motion	534	48.5	-15.9
	After 50 days	544	49.5	1.0

Note: LSR denotes load sharing ratio. Total weight of superstructure-column-raft model is 1100 kN.

3.6 Dynamic bending moment of pile

Figure 20 shows the distribution of maximum bending moments of the corner piles in the two cases. It can be seen that the maximum bending moment is mainly located at the pile head, and the bending moments for pile spacing of 4*d* (Case 2) are relatively larger than 6*d* (Case 1). This may be attributed to the outer piles shielding the internal soil block when using smaller pile spacing. The movement action between the pile and the soil is restrained. In addition, the soil resistance beneath the raft base effectively shares part of the horizontal seismic force when using fewer piles. The contribution of raft contact with soil can play a positive role in earthquake resistance.

Figure 21 shows the maximum bending moments at the pile head for different rows of piles. In general, when the pile spacing is 4*d*, the moment at the pile head is closely related to the pile position. The bending moments of the external rows of piles (such as P1 and P3) that are perpendicular to the shaking direction are generally greater than that of the internal rows of piles (such as P2 and P4). When the pile spacing reaches 6*d*, the horizontal interaction between neighboring piles is reduced, which results in more even distribution of bending moments at each pile head.

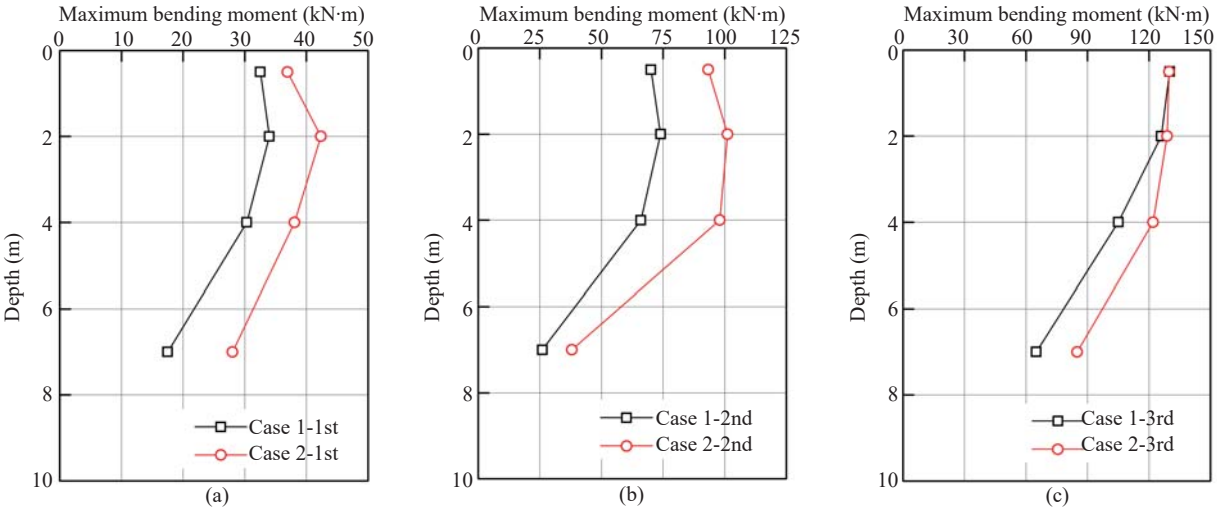

Fig. 20 Maximum bending moment profile along corner pile

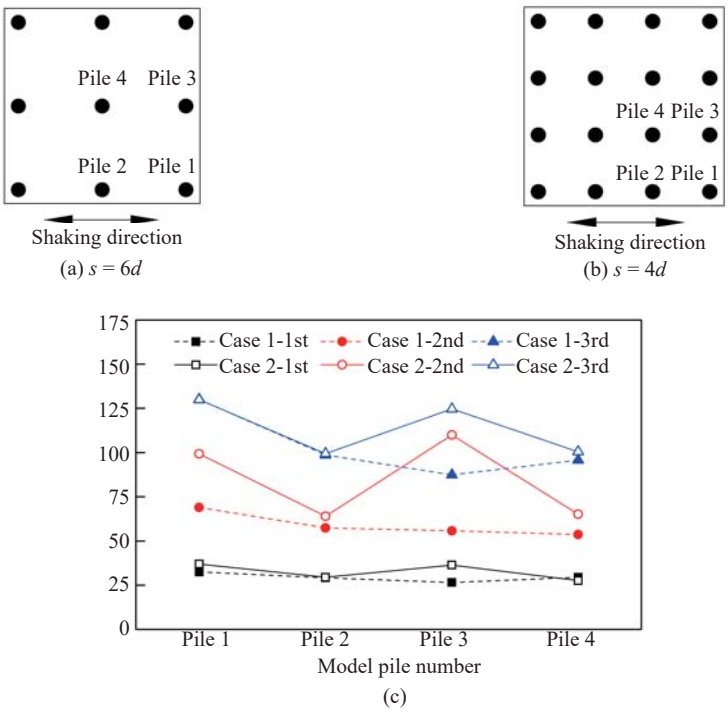

Fig. 21 Maximum bending moments at the pile head

4 Conclusions

(1) The measured soil acceleration results show that it is very effective to simulate the dynamic soil-structure interaction problem with a laminar shear model box. The horizontal motion of soft clay is generally consistent with the results of free-field soil obtained by the equivalent linear model. Soil stress state (consolidation characteristics) and thickness have important effects on the seismic acceleration response of soft ground. The middle soil with low strength tends to play the role of seismic absorption and isolation in the upward transmission of seismic waves. In the natural frequency ranges of soft soil, the spectral acceleration amplification effects are most significant.

(2) In the present test, the seismic acceleration responses of rafts are greater than the surrounding soil surface in most period ranges. With the increase of frequency and level of the input ground motion, the natural period of soft ground and the resonance period of the superstructure-foundation system are both lengthened. The dynamic response of the structure does not necessarily get worse when using fewer piles. On the contrary, the spectral acceleration amplification and the peak acceleration of the superstructure are much lower for the piled raft with larger pile spacing.

(3) Horizontal earthquakes cause superstructure rocking and uneven foundation settlement. The raft instant settlements for both cases are close after the three earthquakes, while the residual lateral displacements and foundation inclination for spacing of 6*d* are generally smaller than 4*d* at the end of the earthquake. In the period of time after the earthquake, the settlement of the foundation continues to occur as a result of soft soil reconsolidation and dissipation of pore water pressure. Using more piles can better control raft settlement after the earthquake, but pile axial forces are more susceptible to increase due to negative friction induced by ground settlement. Benefiting from the dynamic pile-soil-raft interaction, reducing the number of piles is not necessarily unfavorable to displacement control in soft clay under earthquake loading.

(4) Successive earthquakes lead to strain softening and stiffness degradation behavior of soft clay, thereby causing a loss of bearing capacity of the pile raft foundation. Some load transfers from the piles to the raft at the end of each earthquake. However, the total bearing capacity of the pile groups will partially recover following the soil post-earthquake consolidation process. For the piled raft with spacing of 6*d*, the load sharing of piles and raft does not change as much before and after each earthquake. The pile maximum bending moment is not significantly increased when compared to the piled raft with spacing of 4*d*. The maximum bending moments for corner, side and center piles are generally smaller, and the distribution of maximum bending moments at the pile head is more uniform when using larger spacing.

This study provides a useful reference for understanding the seismic response of piled raft in deep soft ground. It should be noted here that the above findings were obtained based on some simplification of the test conditions. For more sophisticated superstructure systems and piled raft foundations, the conclusions of this study will need to be further confirmed through additional testing and detailed analysis.

Acknowledgement

Support from the National Natural Science Foundation of China (No. 41372274) is gratefully acknowledged.

References

Banerjee S, Goh SH and Lee FH (2007), "Response of Soft Clay Strata and Clay–Pile–Raft Systems to Seismic Shaking," *Journal of Earthquake and Tsunami*, **1**(3): 233–255.

Banerjee S, Goh SH and Lee FH (2014), "Earthquake–induced Bending Moment in Fixed-head Piles in Soft Clay," *Geotechnique*, **64**(6): 431–446.

Bemben SM, Myers HJ (1974), "The Influence of Rate of Penetration on Static Cone Resistance in Connecticut River Valley Varved Clay," *Proc., European Symp. on Penetration Testing*, Stockholm: National Swedish Council for Building Research, **2**(2): 33–43.

Chung SF, Randolph MF, Schneider JA (2006), "Effect of Penetration Rate on Penetrometer Resistance in Clay," *Journal of geotechnical and geoenvironmental engineering*, **132**(9): 1188–1196.

Dash SR, Govindaraju L and Bhattacharya S (2009), "A Case Study of Damages of the Kandla Port and Customs Office Tower Supported on a Mat–Pile Foundation in Liquefied Soils Under the 2001 Bhuj Earthquake," *Soil Dynamics and Earthquake Engineering*, **29**: 333–346.

DGJ08-9-2013 (2013), *Code for Seismic Design of Buildings of Shanghai*. (in Chinese)

Hamada J (2016), "Bending Moment of Piles on Piled Raft Foundation Subjected to Ground Deformation During Earthquake in Centrifuge Model Test," *Japanese Geotechnical Society Special Publication*, **2**(34): 1222–1227.

Hamada J, Tanikawa T, Onimaru S, *et al*. (2012), "Seismic Observations on Piled Raft Foundation with Ground Improvement Supporting a Base–Isolated Building," *Proceedings of the 15th WCEE*, Lisboa, Portugal.

Hardin BO and Drnevich VP (1972), "Shear Modulus and Damping in Soils: Measurement and Parameter Effects," *J. Soil Mech. Found. Div.*, ASCE, **98**(6): 603–624.

Hashash YMA, Musgrove MI, Harmon JA, *et al*. (2015), *DEEPSOIL 6.0, User Manual*, pp.104.

Horikoshi K, Matsumoto T, Hashizume Y, *et al*. (2003), "Performance of Piled Raft Foundations Subjected to Dynamic Loading," *International Journal of Physical Modelling in Geotechnics*, **3**(2): 51–62.

Ma K, Banerjee S, Lee FH, *et al*. (2012), "Dynamic Soil–Pile–Raft Interaction in Normally Consolidated Soft Clay During Earthquakes," *Journal of Earthquake and Tsunami*, **6**(3): 1250031.

Ma XF, He ZM, Zhu HH, *et al*. (2006), "Development of a New Geotechnical Centrifuge at Tongji University in Shanghai," *Proc. 6th IC Physical Modelling in Geotechnics*, 2006: 151–156.

Matsuda H and O-Hara S (1990), "Geotechnical Aspects of Earthquake–induced Settlement of Clay Layer," *Marine Georesources and Geotechnology*, **9**(3): 179–206.

Matsumoto T, Fukumura K, Horikoshi K, *et al*. (2004), "Shaking Table Tests on Model Piled Rafts in Sand Considering Influence of Superstructures," International *Journal of Physical Modelling in Geotechnics*, **4**(3): 21–38.

Mendoza MJ, Romo MP, Orozco M, et al. (2000), "Static and Seismic Behavior of a Friction Pile–Box Foundation in Mexico City Clay," *Soils and Foundations*, **40**(4): 143–154.

Nakai S, Katoa H, Ishida R, *et al*. (2004), "Load Bearing Mechanism of Piled Raft Foundation During Earthquake," *Proceedings of 3rd UJNR Workshop on Soil-Structure Interaction*, 2004, Menlo Park, California, USA: 1–18.

Poulos HG (2001), "Piled Raft Foundations: Design and Applications," *Geotechnique*, **51**(2): 95–113.

Saha R, Haldar S and Dutta SC (2015), "Influence of Dynamic Soil–Pile Raft–Structure Interaction: an Experimental Approach," *Earthquake Engineering and Engineering Vibration*, **14**(4): 625–645.

Schofield AN (1981), "Dynamic and Earthquake Geotechnical Centrifuge Modelling," *Proceedings International Conference on Recent Advances in Geotechnical Earthquake Engineering and Soil Dynamics*, Rolla, **3**: 1081–1100.

Scholl RE (1989), "Observations of the performance of buildings during the 1985 Mexico earthquake, and structural design implications," *International Journal of Mining and Geological Engineering*, **7**(1): 69–99.

Stringer ME and Madabhushi SPG (2013), "Re–mobilization of Pile Shaft Friction After an Earthquake," *Canadian Geotechnical Journal*, **50**(9): 979–988.

Tang L, Ling XZ, Xu PJ, *et al*. (2010), "Shake Table Test of Soil–Pile Groups–Bridge Structure Interaction in Liquefiable Ground," *Earthquake Engineering and Engineering Vibration*, **9**(1): 39–50.

Tamura S and Hida T (2014), "Pile Stress Estimation Based on Seismic Deformation Method with Embedment Effects on Pile Caps," *Journal of Geotechnical and Geoenvironmental Engineering*, **140**(9): 04014049.

Tang L, Zhang XY, Ling XZ, *et al*. (2016), "Experimental and Numerical Investigation on the Dynamic Response of Pile Group in Liquefying Ground," *Earthquake Engineering and Engineering Vibration*, **15**(1): 103–114.

Tang YJ, Pei J and Zhao XH (2014), "Design and Measurement of Piled–Raft Foundations," *Proceedings of the Institution of Civil Engineers-Geotechnical Engineering*, **167**(5): 461–475.

Vucetic M and Dobry R (1991), "Effect of Soil Plasticity on Cyclic Response," *Journal of Geotechnical Engineering*, **117**(1): 89–107.

Yamada T, Yamashita K, Kakurai M, et al. (2001), "Long–Term Behaviour of Tall Building on Raft Foundation Constructed by Top–Down Method," *Proceedings of the 5th International Conference on Deep Foundation Practice*, Singapore: 411–417.

Yamashita K, Hamada J and Tanikawa T (2016), "Static and Seismic Performance of a Friction Piled Raft Combined with Grid-Form Deep Mixing Walls in Soft Ground," *Soils and Foundations*, **56**(3): 559–573.

Yamashita K, Hamada J, Wakai S, *et al*. (2014), "Settlement and Load Sharing Behavior of Piled Raft Foundations Based on Long-Term Monitoring," *Takenaka Technical Research Report*, **70**: 29–40.

Yang M (2000), "Study on Reducing–Settlement Pile Foundation Based on Controlling Settlement Principle," *Chinese Journal of Geotechnical Engineering*, **22**(4): 481–486.

Yang M and Yang J (2016), "Centrifuge Investigation on Seismic Response of Piled Raft Foundation with Large Spacing in Soft Clay," *Chinese Journal of Geotechnical Engineering*, **38**(12): 2184–2193. (in Chinese)

Zhang L, Goh SH and Liu HB (2017), "Seismic Response of Pile–Raft–Clay System Subjected to a Long–Duration Earthquake: Centrifuge Test and Finite Element Analysis," *Soil Dynamics and Earthquake Engineering*, **92**: 488–502.

Zhang L, Goh SH and Yi J (2017), "A Centrifuge Study of The Seismic Response of Pile –Raft Systems Embedded in Soft Clay," *Geotechnique*, **67**(6): 479–490.